Research Square

Preprints are preliminary reports that have not undergone peer review.
They should not be considered conclusive, used to inform clinical practice,
or referenced by the media as validated information.

PAK1 Maintains Hepatic Lipid Homeostasis by Modulating PPARγ Phosphorylation and Nuclear Translocation to Attenuate MASLD

Kai Wang

kaiw3@zju.edu.cn

School of Clinical Medicine, Hangzhou Medical College https://orcid.org/0000-0003-4152-8752

Hanzhi Xu

Zhejiang Cancer Hospital, Hangzhou Institute of Medicine

Xun Qiu

Organ Transplant Center, The First Affiliated Hospital, Sun Yat-sen University

Lijun Meng

Key Laboratory of Integrated Oncology and Intelligent Medicine of Zhejiang Province, Hangzhou

Fengqiang Gao

Affiliated Hangzhou First People's Hospital, Zhejiang University School of Medicine

Libin Dong

Zhejiang University School of Medicine

Xin Hu

Zhejiang University School of Medicine

Yawen Tan

Zhejiang University School of Medicine

Nasha Qiu

Key Laboratory of Integrated Oncology and Intelligent Medicine of Zhejiang Province, Affiliated Hangzhou First People's Hospital, School of Medicine, Westlake University

Hao Xu

Department of Hepatobiliary Surgery, The First Affiliated Hospital of Zhejiang Chinese Medical University, Zhejiang Provincial Hospital of Chinese Medicine

Zhan Lixing

Shanghai Institute of Nutrition and Health, Shanghai Institutes for Biological Sciences, University of Chinese Academy of Sciences, Chinese Academy of Science

Xiao Xu

Hepatobiliary Center, The First Affiliated Hospital of Nanjing Medical University https://orcid.org/0000-0002-2761-2811

Article

Keywords: p21-activated kinase 1, Peroxisome proliferator-activated receptor γ, Metabolic dysfunction-associated steatotic liver disease, Metabolic dysfunction-associated steatohepatitis

Posted Date: November 23rd, 2026

DOI: https://doi.org/10.21203/rs.3.rs-11531987/v1

License: This work is licensed under a Creative Commons Attribution 4.0 International License.
Read Full License

Additional Declarations: (Not answered)

Title:

PAK1 Maintains Hepatic Lipid Homeostasis by Modulating PPARγ Phosphorylation and Nuclear Translocation to Attenuate MASLD

Running Title:

Kinase Control of Hepatic Lipid Homeostasis

Authors: Hanzhi Xu[1,2,#], Xun Qiu[3,2#], Lijun Meng[4,#], Fengqiang Gao[2,#], Libin Dong[5], Xin Hu[6], Yawen Tan[2], Nasha Qiu[4], Hao Xu[7,8,*], Lixing Zhan[9,*], Xiao Xu[6,2,*], Kai Wang[10,*]

[*]Corresponding author.

[#] These authors contributed equally to this work.

[1]Zhejiang Cancer Hospital, Hangzhou Institute of Medicine, Chinese Academy of Sciences, Hangzhou 310022, China.

[2]Zhejiang University School of Medicine, Hangzhou 310058, China.

[3]Organ Transplant Center, The First Affiliated Hospital, Sun Yat-sen University, Guangzhou 510080, China.

[4]Key Laboratory of Integrated Oncology and Intelligent Medicine of Zhejiang Province, Affiliated Hangzhou First People's Hospital, School of Medicine, Westlake University, Hangzhou 310006, China.

[5]Institute of Translational Medicine, Zhejiang University School of Medicine, Hangzhou 310000, China.

[6]Hepatobiliary Center and Transplantation Center, The First Affiliated Hospital with Nanjing Medical University, Nanjing 210029, China.

[7]Department of Hepatobiliary Surgery, The First Affiliated Hospital of Zhejiang Chinese Medical

University, Zhejiang Provincial Hospital of Chinese Medicine, Hangzhou 310006, China.

[8]The First School of Clinical Medicine, Zhejiang Chinese Medical University, Hangzhou 310006, China.

[9]Shanghai Institute of Nutrition and Health, University of Chinese Academy of Sciences, Chinese Academy of Sciences, Shanghai 200031, China.

[10]School of Clinical Medicine, Hangzhou Medical College, Hangzhou 314408, China.

Correspondence to: Kai Wang, E-mail: kaiw3@zju.edu.cn

Xiao Xu, E-mail: zjxu@zju.edu.cn

Lixing Zhan, E-mail: lxzhan@sinh.ac.cn

Hao Xu, E-mail: amoyxu@126.com

Abstract:

Metabolic dysfunction-associated steatotic liver disease (MASLD) imposes a substantial global health burden, yet effective interventions remain limited. A previously unrecognized protective role for p21-activated kinase 1 (PAK1) in hepatic lipid metabolism is identified. Hepatic PAK1 expression is elevated in livers affected by MASLD. Lipid overload disrupts the interaction between PAK1 and the ubiquitin ligase tripartite motif-containing protein 21 (TRIM21), thereby reducing PAK1 ubiquitination and proteasomal degradation. PAK1 deficiency exacerbates hepatic lipid accumulation and liver injury, whereas PAK1 overexpression protects against steatosis, inflammation and fibrosis. Mechanistically, PAK1 interacts with peroxisome proliferator-activated receptor gamma (PPARγ) through tyrosine 116 and promotes its inhibitory phosphorylation at serine 112. This phosphorylation limits PPARγ nuclear accumulation and cluster of differentiation 36 (CD36)-dependent fatty acid uptake. Pharmacological PAK1 activation with fingolimod ameliorates established diet-induced MASLD. These findings establish the PAK1/PPARγ axis as an adaptive pathway that restrains hepatic lipid accumulation and support PAK1 activation as a potential therapeutic strategy for MASLD.

Keywords: p21-activated kinase 1; Peroxisome proliferator-activated receptor γ; Metabolic dysfunction-associated steatotic liver disease; Metabolic dysfunction-associated steatohepatitis

1. Introduction

Metabolic dysfunction-associated steatotic liver disease (MASLD) has emerged as the most prevalent chronic liver disease worldwide, with an estimated global prevalence of 32.4%[1]. MASLD is defined by hepatic steatosis in the presence of at least one of five cardiometabolic risk factors.[2]. In a subset of patients, MASLD progresses to metabolic dysfunction-associated steatohepatitis (MASH), increasing the risk of fibrosis, cirrhosis, and hepatocellular carcinoma (HCC)[3-6]. MASLD also imposes a substantial extrahepatic burden and is associated with increased risks of cardiovascular disease, diabetes, and other metabolic disorders, collectively contributing to excess morbidity and mortality[7-9]. Unfortunately, FDA-approved therapies remain limited, particularly for preventing disease onset and broadly arresting its progression[10]. A more comprehensive understanding of the mechanisms underlying MASLD/MASH and the identification of actionable molecular targets therefore remain important priorities.

P21-activated kinase 1 (PAK1) is involved in diverse cellular signaling processes[11]. Loss of Cdc42, a well-established upstream regulator of PAK1, promotes excessive hepatic lipid accumulation[12]. Moreover, PAK1 knockdown disrupts cellular NAD^+/NADH and $NADP^+$/NADPH homeostasis, increases reactive oxygen species (ROS) levels, and impairs mitochondrial function which is integral to lipid metabolism[13]. Another study showed that lipids, especially phosphoinositide, can serve as allosteric regulators of PAK1 and is necessary for its membrane recruitment and activation[14]. Reduced activation of PAK1 and Rac1 in human skeletal muscle has been associated with type 2 diabetes (T2D) and obesity, both of which are closely linked to MASLD pathogenesis[15]. PAK1 also supports insulin-stimulated GLUT4 translocation and contributes to glucose homeostasis and tissue crosstalk with pancreatic β-cells.[16] Collectively, these observations link

PAK1 to multiple metabolic processes relevant to MASLD. However, its direct role in hepatic lipid metabolism and its contribution to MASLD/MASH remain poorly understood.

Peroxisome proliferator-activated receptor γ (PPARγ) is a nuclear receptor that modulates lipid homeostasis including adipogenesis, adipose development, and metabolism [17,18]. PPARγ exerts regulatory effects on lipid through promoting uptake of systematic fatty acids from adipose tissues and fatty acid synthesis via de novo lipogenesis (DNL), leading to increased triglyceride in hepatocytes[19]. Hepatocyte PPARγ knockout reduced MASH progression and hepatic fibrosis[20]. Another study suggested that the PPARγ antagonist GW9662 attenuates the development of diet-induced MASLD[21]. PPARγ activity is tightly and precisely regulated, with posttranslational modifications of the PPARγ protein playing an irreplaceable role. Recent studies have provided growing evidence that PPARγ phosphorylation at distinct sites is essential for regulating its activity and physiological functions. Tissue injury-induced repair signaling reduces PPARγ Thr166 phosphorylation in macrophages, enhancing the binding of PPARγ to the regulatory regions of lipid synthesis genes, thereby augmenting cellular lipogenesis[22]. Besides, Ser112 is currently the only known site where phosphorylation strongly inhibits PPARγ's adipogenic activity[23]. In short, detecting new mechanism of PPARγ regulation will bring light to MASLD/MASH patients.

In this study, we identify PAK1 as an adaptive protective regulator of hepatic lipid metabolism in MASLD. Hepatic PAK1 expression was increased in MASLD due to its weakened interaction with the E3 ubiquitin ligase TRIM21 and limited proteasomal degradation. PAK1 restrained hepatic lipid accumulation, inflammation, and liver injury. Mechanistically, PAK1 combined with PPARγ through Tyr116 and promoted its phosphorylation at Ser112, which restricting PPARγ nuclear accumulation and CD36-dependent fatty acid uptake. Pharmacological activation of PAK1 with

fingolimod ameliorated established diet-induced MASLD. Together, these findings define the PAK1、PPARγaxis as a protective pathway against MASLD and support PAK1 activation as a potential therapeutic strategy.

2. Subjects and Methods

2.1 Cell lines and cell culture

AML12 and HepG2 cell line were purchased from Shanghai Institute of Cell Biology (China) and cultured at 37℃ in an atmosphere containing 5% CO_2 in high glucose DMEM (Gibco, USA) supplemented with 10% fetal bovine serum (Wisent, Canada) and 100 μg/mL penicillin/streptomycin (Invitrogen, USA).

2.2 Regeants

The PAK1 inhibitor FRAX597, PPARγ inhibitor GW9662, PPARγ agonist rosiglitazone, CD36 inhibitor sulfosuccinimidyl oleate, oleic acid, cycloheximide, Fingolimod and MG132 were purchased from MedChem Express (USA).

2.3 MASLD/MASH animal model

Six weeks-old male C57BL/6 mice were obtained from the Animal Facility of Zhejiang University. They were fed high fat diet (HFD, 60 kcal% fat) for 12 weeks or a methionine-choline-deficient diet (MCD) for 6 weeks to establish a MASLD or MASH model, respectively. Subsequently, mice were euthanized, and blood samples and liver tissues were collected. The experimental protocols were authorized by the Institutional Animal Care and Use Commite (IACUC) ZJCLA.

2.4 Real-time quantitative PCR analysis

Total RNA was extracted from cells using TRIzol reagent (Invitrogen, USA) according to the manufacturer's instructions. RNA was reverse-transcribed into cDNA using HiScript II RT SuperMix for qPCR (+gDNA wiper; Vazyme, China). Quantitative real-time PCR was performed using ChamQ SYBR Color qPCR Master Mix (Vazyme, China) on a CFX96 Touch Real-Time PCR Detection System (Bio-Rad, CA, USA). Relative transcript abundance was calculated from threshold cycle (Ct) values and normalized to β-actin. The primer sequences are provided in Supporting Table S1.

2.5 Western blotting analysis

Cells and mouse liver tissues were lysed in RIPA buffer (FUDE, China) supplemented with protease and phosphatase inhibitors. Lysates were incubated on ice for 30 min and clarified by centrifugation at 14,000 × g for 10 min at 4 °C. The supernatants were collected, and protein concentrations were determined using a BCA assay (FUDE, China). Proteins were separated by SDS–PAGE and transferred onto PVDF membranes using a wet-transfer system. The membranes were blocked with 5% skim milk and incubated with primary antibodies overnight at 4 °C, followed by secondary antibodies for 1–2 h at room temperature. Protein bands were visualized by chemiluminescence. Antibody information is provided in Supporting Table S2.

2.6 Immunohistochemistry staining

Liver tissues were fixed in 4% paraformaldehyde, dehydrated through a graded series, embedded in paraffin, and sectioned. Endogenous peroxidase activity was quenched with 3% H_2O_2 for 10 min. Nonspecific binding was blocked with 10% BSA for 1 h at 37 °C. Sections were incubated with the indicated primary antibodies (Servicebio, China) overnight at 4 °C, followed by biotinylated secondary antibodies (Millipore, USA) for 1 h at 37 °C. The sections were then

incubated with HRP-conjugated avidin (Vector Laboratories, USA) for 30 min. Immunoreactivity was visualized using 3,3′-diaminobenzidine (Zhongshan Golden Bridge Biological Technology Co., Ltd., China), and nuclei were counterstained with hematoxylin. Stained sections were examined and imaged using a light microscope.

2.7 Hematoxylin and Eosin staining and Sirius Red staining

Liver tissues were fixed in 4% paraformaldehyde, dehydrated, and embedded in paraffin. Paraffin-embedded tissues were cut into 4 μm sections, deparaffinized in xylene, and rehydrated through a graded ethanol series. Sections were stained with hematoxylin and eosin (H&E) or Sirius Red and imaged using a light microscope.

2.8 Oil Red O staining

For cellular Oil Red O staining, cells were fixed with 4% paraformaldehyde for 15 min, washed with PBS, and incubated in 60% isopropanol for 5 min. Cells were stained with Oil Red O (Sigma-Aldrich, USA) for 30 min at room temperature and counterstained with hematoxylin for 30 s. Images were acquired using an Olympus digital camera.

For tissue staining, liver samples were embedded in optimal cutting temperature (OCT) compound, frozen, and sectioned at 8–10 μm using a cryostat. Cryosections were fixed with 4% paraformaldehyde for 10–15 min, rinsed with distilled water, and equilibrated in 60% isopropanol. Sections were stained with freshly prepared Oil Red O working solution for 10–15 min and briefly differentiated in 60% isopropanol to reduce background staining. After rinsing with distilled water, nuclei were counterstained with hematoxylin. Sections were mounted using an aqueous mounting medium and examined under a light microscope..

2.9 TG, TC, LDL-C measurement and liver function assays

Triglyceride (TG), total cholesterol (TC), low-density lipoprotein cholesterol (LDL-C), alanine aminotransferase (ALT), and aspartate aminotransferase (AST) were measured using commercial assay kits (Jiancheng Bio, China) according to the manufacturer's instructions.

2.10 Nuclear and cytoplasmic protein fractionation

Nuclear and cytoplasmic proteins were isolated using a nuclear/cytoplasmic protein extraction kit according to the manufacturer's instructions. All procedures were performed on ice or at 4 °C. Adherent cells were washed with ice-cold PBS, harvested by scraping, and pelleted by centrifugation. Cell pellets were incubated in cytoplasmic lysis buffer supplemented with protease and phosphatase inhibitors. After membrane disruption and centrifugation, the supernatants were collected as the cytoplasmic fractions. The remaining nuclear pellets were washed, lysed in nuclear extraction buffer, and subjected to high-speed centrifugation. The resulting supernatants were collected as the nuclear fractions. Protein fractions were stored at −80 °C until further analysis.

2.11 Glucose tolerance test

Mice were fasted for 12–16 h with access to water. Glucose was administered intraperitoneally at 2 g/kg body weight. Blood glucose concentrations were measured in tail-vein blood using a glucometer at baseline (0 min) and 15, 30, 60, and 120 min after glucose administration. Glucose tolerance was evaluated by calculating the area under the glucose–time curve (AUC).

2.12 Adeno-associated-virus 8 vectors construction

AAV8 vectors for PAK1 knockdown or overexpression were generated by Hanbio (China). Control mice received the corresponding empty AAV8-TBG vector. Each mouse was administered 3×10^{11} vector genomes (vg) in a total volume of 100 μL via tail-vein injection.

2.13 Lentivirus infection, plasmid and siRNA transfection

The corresponding lentivirus outputs of these expression plasmids (Genechem, China) were infected into cells with polybrene (Sigma-Aldrich, USA) assistance to obtain favorable effects. For screening stable cell line, cells were infected with the corresponding lentivirus outputs for 72 h, and then the selective medium containing puromycin (Sigma-Aldrich, USA) with final concentration 2 μg/ml was added and replaced every 2 days. Plasmid expressing PPARγ, PPARγ S112A or Y116A (Genechem，China) and siRNA of PAK1(GenePharma, China) were transfected into cells with polybrene (Polyplus Transfection, France) after cells were seeded in six-well plates and reached 70% confluence according to the manufacture's instruction. The sequences of siRNA are listed in Supporting Table S3.

2.14 Bulk RNA-seq

The control and PAK1-OE AML12 cells after 24h 400 μM oleic acid treatment were put into TRIzol (Invitrogen, USA) and then quickly transported into liquid nitrogen for subsequent mRNA sequencing under customized service of Tsingke BioTechnology (Tsingke, China). After the final transcriptome was generated, bioinformatic analysis was performed using the tools at https://cloud.tsingke.com.cn. The genes with $P < 0.05$ were considered differentially expressed genes. Differentially expressed genes were then subjected to enrichment analysis of KEGG, GO and GSEA.

2.15 Fatty acid uptake assay

Cells were seeded in 96-well plates and serum-starved for 8 h. The cells were incubated with BODIPY-FA (Thermo Fisher Scientific, USA) for 30 min at 37 °C, washed twice with PBS, and

fixed with 4% paraformaldehyde. Fluorescence images were acquired using an Olympus fluorescence microscope.

2.16 Immunoprecipitation and mass spectrometry analysis

Cells were lysed in RIPA buffer (FUDE, China). Cell lysates were incubated with 1–2 μg of the indicated antibody for 2 h at 37 °C with rotation. Protein A/G agarose beads (Thermo Fisher Scientific, USA) were added, and the samples were rotated for an additional 1 h. The immunoprecipitates were washed three times with PBST for 10 min per wash. Whole-cell lysates and immunoprecipitated proteins were analyzed by western blotting. To identify PAK1-interacting proteins, protein-containing gel slices were submitted to Omicsolution (China) for liquid chromatography–mass spectrometry (LC–MS) analysis.

2.17 Chromatin immunoprecipitation assay

Chromatin immunoprecipitation (ChIP) was performed using a ChIP Assay Kit (Beyotime, China) according to the manufacturer's instructions. Cells were crosslinked with 1% formaldehyde for 10 min at 37 °C, and the reaction was quenched with glycine for 5 min at room temperature. After washing with ice-cold PBS containing PMSF, the cells were harvested and lysed on ice. Chromatin was sheared by sonication to generate DNA fragments of 200–1,000 bp. Following centrifugation, the soluble chromatin was collected, diluted, and precleared with magnetic beads. An aliquot was retained as the input control, while the remaining chromatin was incubated with the indicated antibody overnight at 4 °C. The immune complexes were captured with magnetic beads, sequentially washed, and eluted with SDS/$NaHCO_3$ buffer. Crosslinks were reversed at 65 °C, followed by proteinase K digestion and DNA purification. The purified DNA was analyzed by PCR.

2.18 Theoreticl modelling and molecular dynamics (MD) simulations

AlphaFold-multimer was used to predict the complex formed by mouse PAK1 and its substrate. For the substrate, peptide segments having different lengths (11, 15 and 21 residues) and with phosphorylation site Ser112 as the center residue were, respectively, used as input for predictions[24]. Among all generated complexes, the ones, wherein the hydroxyl group of Ser112 is near to the γ phosphate group of ATP, were assumed to hold reasonable binding modes and therefore selected to construct systems for subsequent MD simulations.

Since there is no experimentally resolved crystal structure of mouse PAK1 in complex with ATP and metal ions, but exists crystal structure of human PAK1 (PDB: 3Q53) in complex with ATP and metal ions, and they are a pair of highly homologous proteins. We added ATP and metal ions into the catalytic pocket of mouse PAK1 by aligning the backbone atoms of mouse PAK1 with those of human PAK1. In addition, Thr423 was phosphorylated using CHARMM-GUI to mimic the active state of PAK1[25,26].

The systems for MD simulations were constructed and simulated using the package GROMACS[27]. The obtained trajectories were analyzed using VMD software[28]. The complex was solvated with a 150 mM NaCl electrolyte. We applied the CHARMM36 force field for protein and ions, the TIP3P model for water molecules. The forcefields of ATP was generated using CGenFF[29,30]. The simulation time step is 2 fs. The pairwise vdW interaction was calculated using a smooth (0.10 - 0.12 nm) cutoff. The long-range Coulomb interaction was computed using the particle-mesh Ewald method with a mesh size of 0.1 nm. Production runs were performed in NPT ensembles. The pressure was kept at 1 bar using isotropic Parrinello-Rahman pressostat. The temperature was kept at 310K by applying the Nose-Hoover thermostat.

2.19 Statistical analysis

All quantitative data are presented as the mean ±SD of at least three independent experiments. Student's t-test was used for comparison between two groups, and one way ANOVA plus post hoc test was utilized for comparison between more than two groups. A value of $p<0.05$ was considered statistically significant. Statistical analysis was performed using GraphPad Prism (version 8.0.1).

3. Results

3.1 PAK1 expression is increased in livers and hepatocytes with steatosis

To investigate the potential involvement of PAK1 in MASLD progression, we first analyzed publicly available datasets from the Gene Expression Omnibus (GEO). Hepatic PAK1 expression was significantly higher in patients with simple steatosis or NASH than in healthy controls (Fig. 1a). Consistent with this finding, an independent dataset showed markedly elevated hepatic PAK1 mRNA levels in patients with NAFLD or NASH compared with normal individuals (Fig. 1b).

We next examined PAK1 expression in vitro by treating AML12 and HepG2 cells with oleic acid (OA) for up to 24 h. OA treatment significantly increased PAK1 mRNA and protein levels in both cell lines. The abundance of phosphorylated PAK1 (pPAK1), the activated form of PAK1, was also markedly increased (Fig. 1c–f).

We further assessed hepatic PAK1 expression in dietary mouse models. Consistent with the in vitro findings, mice fed either a high-fat diet (HFD) or a methionine-choline-deficient diet (MCD) exhibited significantly increased hepatic PAK1 mRNA and protein levels compared with normal-diet-fed controls (Fig. 1g–j). Immunohistochemical analyses further confirmed increased PAK1 expression and phosphorylation in the livers of HFD- and MCD-fed mice (Fig. 1k,l).

Collectively, these findings demonstrate consistent upregulation and activation of PAK1 across

human datasets and experimental models of MASLD/MASH, supporting its potential involvement in disease progression.

3.2 PAK1 suppresses lipid accumulation in steatotic hepatocytes

To define the functional role of PAK1 in hepatocellular steatosis, we designed PAK1-targeting siRNAs and confirmed their knockdown efficiency by western blotting (Fig. 2a). PAK1 silencing increased lipid accumulation in OA-treated AML12 cells (Fig. 2b,c). PAK1 depletion also increased the expression of genes involved in lipid synthesis and uptake, including Scd1, Cd36, Pparg, and Acaca. Conversely, the expression of genes associated with fatty acid β-oxidation, including Cpt1a and Ppara, was reduced (Fig. 2d).

We subsequently generated AML12 cells stably overexpressing PAK1 and confirmed PAK1 overexpression (Fig. 2e). In contrast to PAK1 knockdown, PAK1 overexpression reduced hepatocellular lipid accumulation (Fig. 2f,g). Consistently, PAK1 overexpression suppressed genes associated with lipogenesis and fatty acid uptake while increasing the expression of genes involved in β-oxidation (Fig. 2h). Similar results were observed in human hepatocytes, supporting a conserved role for PAK1 in the regulation of hepatocellular lipid metabolism (Supplementary Fig. 1a–h).

To characterize the broader transcriptional changes associated with PAK1 overexpression, we performed RNA sequencing of control and PAK1-overexpressing AML12 cells. Transcriptomic analysis identified 1,480 upregulated and 1,387 downregulated genes in PAK1-overexpressing cells relative to control cells (Fig. 2i). The downregulated genes were enriched in lipid metabolic pathways, including fatty acid biosynthesis, triglyceride biosynthesis, and unsaturated fatty acid biosynthesis. By contrast, the upregulated genes were enriched in pathways associated with negative

regulation of immune responses, negative regulation of lipid metabolism, and lipid homeostasis (Fig. 2j,k; Supplementary Fig. 1i). A heatmap further revealed marked differences in the expression of lipid metabolism- and inflammation-related genes between control and PAK1-overexpressing hepatocytes (Fig. 2l).

Collectively, these findings indicate that PAK1 limits lipid accumulation in steatotic hepatocytes. PAK1 overexpression was also associated with broad transcriptional changes in pathways related to lipid metabolism, lipid homeostasis, and immune regulation.

3.3 PAK1 attenuates HFD and MCD diet-induced MASLD/MASH

To determine the in vivo role of PAK1 in MASLD, we generated a model of liver-specific PAK1 overexpression using AAV8-PAK1, with AAV8-NC as the control. Mice received intravenous injections of the indicated viruses and were allowed 2 weeks for hepatic transgene expression before dietary intervention. For the HFD model, mice were subsequently fed a high-fat diet for 12 weeks before sample collection (Fig. 3a). Efficient hepatic overexpression of PAK1 was confirmed (Supplementary Fig. 2a).

PAK1 overexpression significantly reduced liver weight and hepatic triglyceride content compared with the control group (Fig. 3b,c). Histological analysis further showed reduced hepatocellular lipid deposition and fewer lipid droplets (Fig. 3d,e). Serum alanine aminotransferase (ALT) and aspartate aminotransferase (AST) levels were also significantly decreased, consistent with attenuated liver injury (Fig. 3f). By contrast, glucose tolerance remained unchanged (Fig. 3g). Serum triglyceride (TG), total cholesterol (TC), and low-density lipoprotein cholesterol (LDL-C) levels were also unaffected by PAK1 overexpression (Supplementary Fig. 2b). At the molecular level, PAK1 overexpression increased the expression of fatty acid β-oxidation-related genes. Conversely, genes

associated with lipid uptake, de novo lipogenesis, and hepatic inflammation were suppressed under metabolic stress (Fig. 3h).

We next evaluated the effects of PAK1 overexpression in an MCD diet-induced MASH model. Following viral delivery, mice were fed an MCD diet for 6 weeks before sample collection (Fig. 3i). Efficient hepatic PAK1 overexpression was again confirmed (Supplementary Fig. 2c). Although liver weight did not differ significantly between groups, hepatic triglyceride content was markedly reduced in PAK1-overexpressing mice (Fig. 3j,k). H&E and Oil Red O staining also revealed attenuated hepatic steatosis and histological injury in these mice (Fig. 3l,m). Moreover, Sirius Red staining showed that PAK1 overexpression mitigated MCD-induced hepatic fibrosis (Fig. 3n). Consistent with these histological findings, serum ALT and AST levels were significantly decreased, whereas glucose tolerance remained unchanged (Fig. 3o,p). PAK1 overexpression also increased the expression of β-oxidation-related genes while suppressing genes involved in lipid uptake, lipid synthesis, and inflammation (Fig. 3q). Serum TG, TC, and LDL-C levels were not significantly altered in this model (Supplementary Fig. 2d).

To complement these gain-of-function experiments, we silenced hepatic PAK1 in vivo using liver-targeted AAV8-mediated knockdown. Knockdown efficiency was confirmed in both dietary models (Supplementary Fig. 3a; Supplementary Fig. 4a). PAK1 knockdown increased liver weight in HFD-fed mice but had no significant effect on liver weight in MCD-fed mice (Supplementary Fig. 3b; Supplementary Fig. 4b). Hepatic triglyceride accumulation and serum ALT and AST levels were markedly increased following PAK1 knockdown (Supplementary Fig. 3c,d; Supplementary Fig. 4c,d). By contrast, circulating TG, TC, and LDL-C levels remained unchanged (Supplementary Fig. 3e; Supplementary Fig. 4e). Glucose tolerance was also unaffected by PAK1 knockdown

(Supplementary Fig. 3f; Supplementary Fig. 4f). Histological analysis further revealed more pronounced hepatic steatosis following PAK1 knockdown, as shown by H&E and Oil Red O staining (Supplementary Fig. 3g; Supplementary Fig. 4g). Sirius Red staining additionally showed aggravated hepatic fibrosis in MCD-fed mice following PAK1 knockdown (Supplementary Fig. 4g). Collectively, these reciprocal gain- and loss-of-function experiments support a protective role for hepatic PAK1 against diet-induced steatosis and liver injury. They further indicate that PAK1 attenuates pathological features of HFD-induced MASLD and MCD-induced MASH in vivo..

3.4 TRIM21 mediates degradation of PAK1 in liver steatosis

We next investigated the mechanism underlying PAK1 upregulation during hepatic steatosis. Protein half-life assays showed that OA treatment markedly prolonged the half-life of PAK1 (Fig. 4a). This finding suggested that OA-induced lipid overload increased PAK1 abundance, at least partly, by enhancing its protein stability.

Because intracellular proteins are primarily degraded through the ubiquitin–proteasome or autophagy–lysosome pathway, we examined which pathway regulated PAK1 turnover under steatotic conditions. Hepatocytes were treated with the corresponding inhibitors in the presence or absence of OA. Cycloheximide was used to inhibit de novo protein synthesis. The OA-dependent difference in PAK1 abundance was abolished by the proteasome inhibitor MG132 but persisted after treatment with the lysosomal inhibitor chloroquine (Fig. 4b). These results implicated the ubiquitin–proteasome system, rather than the lysosomal pathway, in the regulation of PAK1 stability. Consistently, immunoprecipitation assays showed that OA treatment markedly reduced PAK1 ubiquitination (Fig. 4c). Thus, the increased stability of PAK1 under metabolic stress was associated with reduced ubiquitin-dependent proteasomal degradation.

We further performed immunoprecipitation coupled with mass spectrometry (IP–MS). Candidate interactors were ranked according to their peptide-spectrum match (PSM) scores, identifying TRIM21 as a potential PAK1-interacting protein (Fig. 4d). Co-immunoprecipitation assays subsequently confirmed the interaction between PAK1 and TRIM21. This interaction progressively decreased with increasing OA concentrations (Fig. 4e). To determine whether TRIM21 regulated PAK1 stability, we silenced TRIM21 in hepatocytes using siRNA. TRIM21 knockdown markedly reduced PAK1 ubiquitination and prolonged its protein half-life (Fig. 4f,g). Functionally, TRIM21 depletion attenuated hepatocellular lipid accumulation (Fig. 4h,i).

Collectively, these findings identify TRIM21 as a regulator of PAK1 ubiquitination and stability. They support a model in which lipid overload promotes PAK1 accumulation by weakening TRIM21-dependent ubiquitination and proteasomal degradation.

3.5 PAK1 suppresses lipid accumulation through PPARγ/CD36 pathway

RNA sequencing revealed significant suppression of the PPAR signaling pathway in PAK1-overexpressing hepatocytes (Fig. 5a). Among the PPAR family members, PPARγ regulates hepatocellular fatty acid uptake partly by transactivating the lipid transporter CD36. Consistent with this function, transcriptomic analysis showed that multiple canonical PPARγ target genes were downregulated following PAK1 overexpression (Fig. 5b).Chromatin immunoprecipitation (ChIP) assays further showed that PAK1 overexpression markedly reduced PPARγ occupancy at the CD36 promoter. Conversely, PAK1 knockdown increased PPARγ binding to this region (Fig. 5c).

To determine whether PPARγ mediated the metabolic effects of PAK1, we performed pharmacological rescue experiments. The PPARγ antagonist GW9662 largely abolished the PAK1 knockdown-induced increases in CD36 transcription and fatty acid uptake (Fig. 5d; Supplementary

Fig. 5a). GW9662 also reversed the increase in hepatocellular lipid accumulation caused by PAK1 knockdown (Fig. 5e,f).Conversely, pharmacological activation of PPARγ with rosiglitazone largely counteracted the metabolic effects of PAK1 overexpression. Rosiglitazone restored CD36 expression and fatty acid uptake, both of which were reduced by PAK1 overexpression (Fig. 5g; Supplementary Fig. 5b). Consistently, rosiglitazone reversed the reduction in lipid accumulation conferred by PAK1 overexpression, resulting in renewed intracellular lipid accumulation (Fig. 5h,i). To examine the contribution of CD36 downstream of PPARγ, we inhibited CD36 using either sulfosuccinimidyl oleate (SSO) or siRNA-mediated knockdown. Both interventions markedly blunted the increase in lipid accumulation induced by PAK1 knockdown (Fig. 5j,k; Supplementary Fig. 5c–e).

Collectively, these findings identify the PPARγ/CD36 pathway as a major mediator of PAK1-dependent regulation of hepatocellular lipid accumulation.

3.6 PAK1 binds to PPARγ at Tyr116 to facilitate its phosphorylation at Ser112 and decrease its nuclear disturbution

Building on these findings, we investigated the molecular mechanism through which PAK1 restrains hepatocellular lipid accumulation. Immunoblotting showed that hepatic PAK1 overexpression or pharmacological PAK1 activation with fingolimod reduced nuclear PPARγ abundance. Conversely, PAK1 deficiency increased the nuclear accumulation of PPARγ (Fig. 6a; Supplementary Fig. 6a,b). PAK1 is a serine/threonine kinase, and PPARγ phosphorylation at Ser112 reportedly suppresses its transcriptional activity in other metabolic contexts. We therefore hypothesized that PAK1 regulates PPARγ activity by promoting its phosphorylation at Ser112 (Fig. 6b). PAK1 overexpression markedly increased PPARγ Ser112 phosphorylation in hepatocytes and mouse livers, whereas

PAK1 knockdown reduced Ser112 phosphorylation (Fig. 6c; Supplementary Fig. 6c,d).

To assess the functional importance of this site, we generated constructs encoding wild-type PPARγ or the non-phosphorylatable PPARγ S112A mutant. Expression of both constructs was confirmed by immunoblotting (Fig. 6d). Compared with wild-type PPARγ, the S112A mutant exhibited greater nuclear accumulation and increased promoter occupancy in ChIP assays (Fig. 6e,f). PAK1 suppressed fatty acid uptake in cells expressing wild-type PPARγ, but this effect was largely lost in cells expressing PPARγ S112A (Supplementary Fig. 6e). Similarly, expression of PPARγ S112A substantially reversed the reduction in lipid accumulation induced by PAK1 overexpression (Fig. 6g,h). These findings indicate that PPARγ Ser112 is required for the metabolic effects of PAK1 in hepatocytes.

We next examined whether PAK1 physically interacts with PPARγ. Co-immunoprecipitation assays confirmed an interaction between the two proteins (Fig. 6i). We then performed computational modeling and molecular dynamics (MD) simulations to investigate the structural basis of PPARγ recognition by PAK1.Because Ser112 lies within an intrinsically disordered region, AlphaFold-Multimer was used to model mouse PAK1 bound to PPARγ-derived peptides of different lengths. Each peptide spanned the Ser112-containing region. Candidate complexes were selected according to the spatial relationship between Ser112 and the ATP γ-phosphate within the PAK1 catalytic pocket. The selected models were subsequently subjected to MD simulations to assess their conformational stability. These analyses identified a stable binding mode that positioned the Ser112 hydroxyl group near the ATP γ-phosphate, a configuration compatible with phosphotransfer (Fig. 6j). Further structural analysis predicted that PPARγ Tyr116 functions as an anchoring residue during substrate engagement. Tyr116 inserted into a narrow surface pocket on PAK1 and formed a

hydrogen bond with Glu207 at the base of the catalytic cleft. The distance between these residues remained stable throughout the simulation, with an average separation of 0.36 nm. Moreover, the root-mean-square deviation of the Ser112–Tyr116 peptide segment fluctuated within a narrow range, indicating stable peptide association with PAK1 (Fig. 6k).

To test the functional relevance of this predicted interface, we generated a Tyr116-mutant PPARγ construct and expressed it in AML12 cells. Tyr116 mutation significantly increased the nuclear localization of PPARγ (Fig. 6l). The mutation also attenuated the PAK1–PPARγ interaction and reduced PPARγ phosphorylation, consistent with the structural prediction (Fig. 6m). ChIP assays further showed increased binding of the mutant PPARγ to the CD36 promoter (Fig. 6n). Functionally, the Tyr116 mutant induced greater intracellular lipid accumulation than wild-type PPARγ (Fig. 6o,p).

Collectively, these findings support a model in which PAK1 interacts with PPARγ at Tyr116 and promotes its inhibitory phosphorylation at Ser112.

3.7 PAK1 agonists Fingolimod protects against MASLD/MASH

To evaluate the preclinical therapeutic potential of PAK1 activation in MASLD/MASH, we examined whether fingolimod could ameliorate established diet-induced disease in mice. In the HFD model, mice were fed a high-fat diet for 10 weeks to induce hepatic steatosis. They subsequently received daily intraperitoneal injections of fingolimod or PBS for 2 weeks while HFD feeding was continued (Fig. 7a).

Fingolimod treatment significantly reduced liver weight and hepatic triglyceride content (Fig. 7b,c). H&E staining showed less severe hepatic histopathology, while Oil Red O staining revealed reduced lipid deposition (Fig. 7d,e). Serum alanine aminotransferase (ALT) and aspartate aminotransferase

(AST) levels were also significantly decreased, consistent with attenuated hepatocellular injury (Fig. 7f). By contrast, fingolimod did not significantly affect glucose tolerance (Fig. 7g). At the molecular level, fingolimod increased PAK1 and PPARγ phosphorylation while reducing CD36 protein abundance (Fig. 7h). RT-qPCR analysis showed reduced expression of lipogenic and inflammatory genes and increased expression of genes associated with fatty acid β-oxidation (Fig. 7i).

We next evaluated fingolimod in an MCD diet-induced MASH model. Mice were fed an MCD diet for 4 weeks before receiving daily intraperitoneal injections of fingolimod or PBS. Treatment continued for 2 weeks while MCD feeding was maintained, and mice were analyzed at the end of the 6-week protocol (Fig. 7j).

Fingolimod significantly reduced liver weight and hepatic triglyceride accumulation in MCD-fed mice (Fig. 7k,l). H&E and Oil Red O staining further showed attenuated hepatic injury and lipid accumulation, respectively (Fig. 7m,n). Sirius Red staining also revealed reduced hepatic fibrosis following fingolimod treatment (Fig. 7o). Consistent with these histological findings, serum ALT and AST levels were decreased, whereas glucose tolerance remained unchanged (Fig. 7p,q). Fingolimod again increased hepatic PAK1 and PPARγ phosphorylation (Fig. 7r). It also reduced the expression of genes involved in lipid synthesis and inflammation while increasing fatty acid β-oxidation-related gene expression (Fig. 7s).

Collectively, these findings show that fingolimod ameliorates established diet-induced hepatic steatosis and injury in both HFD- and MCD-fed mice. These improvements were accompanied by increased PAK1 and PPARγ phosphorylation, reduced CD36 abundance, and favorable changes in lipid metabolism- and inflammation-related gene expression. The results support further evaluation of the PAK1/PPARγ axis as a potential therapeutic target for MASLD/MASH.

4 Discussion

Our findings identify PAK1 as a protective regulator of hepatic lipid homeostasis in MASLD/MASH. Lipid accumulation stabilized PAK1 by weakening its association with TRIM21 and reducing ubiquitin-dependent degradation. PAK1 overexpression attenuated hepatic lipid accumulation, inflammation, and fibrosis in diet-induced MASLD models. Mechanistically, PAK1 associated with PPARγ through an interface involving Tyr116 and promoted its phosphorylation at Ser112. This modification reduced nuclear PPARγ accumulation, suppressed CD36 transcription, and limited hepatocellular fatty acid uptake. Together, these findings define a PAK1/PPARγ signaling axis that may be therapeutically relevant to MASLD/MASH.

Previous studies of PAK1 have focused predominantly on its role in glucose metabolism, whereas its involvement in MASLD/MASH remains poorly understood. Excessive hepatic lipid accumulation, arising from an imbalance between lipid synthesis and oxidation, is a central pathological feature of MASLD/MASH[31]. Our findings extend this understanding by identifying a PAK1-dependent mechanism that limits hepatic steatosis. PAK1 overexpression suppressed genes associated with lipid synthesis while increasing the expression of genes involved in fatty acid β-oxidation. These coordinated changes support a role for PAK1 in maintaining hepatic lipid homeostasis.

Excessive lipid accumulation can induce hepatocellular lipotoxicity and promote the release of damage-associated molecular patterns. These signals activate Kupffer cells and hepatic stellate cells, thereby contributing to inflammation and fibrosis, respectively[32,33]. Previous studies showed that PAK1 loss exacerbated inflammation through activation of Notch1 signaling[34]. PAK1 has also been linked to Wnt/β-catenin signaling, which promotes anti-inflammatory M2 macrophage

polarization[35,36]. Consistent with these observations, hepatic PAK1 overexpression attenuated inflammation and liver injury in mice fed either an HFD or MCD diet. The relationship between PAK1 signaling and fibrosis appears to be context dependent. Deletion of CDC42, an upstream regulator of PAK1, accelerated pulmonary fibrosis through activation of TGF-β signaling[37]. Conversely, another study found that loss of PAK1-dependent signaling impaired mechanoadaptive responses and markedly reduced fibrosis[38]. Differences in tissues and experimental models may account for these apparently divergent findings. In our MASH model, hepatic PAK1 overexpression reduced fibrosis, whereas PAK1 knockdown aggravated this phenotype. Further studies are required to determine how PAK1 regulates hepatic stellate cell activation and fibrogenic signaling.

The ubiquitin–proteasome system regulates numerous aspects of cellular physiology by controlling protein abundance and turnover[39,40]. Previous studies reported that ivermectin and BJG-05-039 promote PAK1 degradation through the ubiquitin–proteasome pathway[41-44]. Our results extend these observations by implicating TRIM21, an E3 ubiquitin ligase, in the regulation of PAK1 stability. IP–MS identified TRIM21 as a potential PAK1-interacting protein, and subsequent experiments confirmed their association. Metabolic stress weakened the PAK1–TRIM21 interaction and reduced PAK1 ubiquitination. Moreover, TRIM21 knockdown prolonged the half-life of PAK1. These findings support a model in which reduced TRIM21-dependent degradation contributes to the adaptive accumulation of PAK1 under steatotic conditions.

PPARγ is a ligand-activated nuclear receptor that regulates adipogenesis, metabolism, and immunity[45]. Hepatocellular PPARγ signaling has also been implicated in the initiation and progression of MASLD/MASH. NRF2-dependent induction of PPARγ has been linked to the

development of hepatic steatosis[46]. The HDAC1/PPARγ axis has also been targeted by FA/p-CA to reduce free fatty acid uptake and ameliorate MASLD[47]. CD36 is a PPARγ target and a major mediator of fatty acid uptake, linking hepatic PPARγ activity to MASLD/MASH[48-50]. Our findings position PAK1 upstream of the PPARγ/CD36 pathway. PAK1 overexpression reduced nuclear PPARγ accumulation, CD36 expression, and fatty acid uptake. Conversely, PAK1 knockdown increased each of these measures. Pharmacological modulation of PPARγ reversed the effects of PAK1 overexpression or knockdown on CD36 expression, fatty acid uptake, and lipid accumulation. Inhibition of CD36 similarly attenuated the increase in lipid accumulation caused by PAK1 knockdown. These reciprocal experiments support the PPARγ/CD36 pathway as a major mediator of PAK1-dependent regulation of hepatocellular lipid accumulation. Consistent with this interpretation, GW9662, the PPARγ antagonist used in our in vitro experiments, has been reported to ameliorate MASLD in mice[21]. PPARγ activity is regulated by phosphorylation at several sites, with functional consequences that vary across tissues and metabolic contexts. Inhibition of PPARγ Ser225 phosphorylation alleviates pulmonary arterial hypertension in pulmonary artery smooth muscle cells[51]. Inhibiting Ser273 phosphorylation enhances insulin sensitivity[52], although obesity-associated Ser273 phosphorylation may exert beneficial hepatic effects[53]. Inhibition of Thr166 phosphorylation increases beige adipocyte inducibility and improves metabolic dysfunction[54]. In addition, adipocytes expressing non-phosphorylatable PPARγ S112A show increased sensitivity to ligand-induced adipogenesis[55]. WIP1-mediated dephosphorylation of PPARγ Ser112 similarly promotes pre-adipocyte differentiation[23]. Together, these studies underscore the site- and context-dependent consequences of PPARγ phosphorylation. Our results extend this regulatory framework to hepatocellular lipid metabolism. PAK1 interacted with PPARγ and increased its phosphorylation

at Ser112, whereas PAK1 knockdown reduced this modification. The PPARγ S112A mutant showed increased nuclear accumulation and promoter occupancy. This mutation also substantially diminished the effects of PAK1 on fatty acid uptake and lipid accumulation. These findings indicate that Ser112 is functionally required for PAK1-dependent regulation of PPARγ. Structural modeling further suggested that PPARγ Tyr116 participates in substrate recognition by PAK1. However, the precise enzymatic mechanism underlying this phosphorylation remains to be fully defined.

We further evaluated the therapeutic relevance of this pathway using fingolimod. Fingolimod (FTY720) is an oral, first-in-class sphingosine-1-phosphate receptor modulator that received FDA approval in 2010 for relapsing forms of multiple sclerosis in adults. Pivotal phase III trials demonstrated that fingolimod reduced annualized relapse rates compared with placebo or intramuscular interferon β-1a[56,57]. Thus, fingolimod is a clinically available, FDA-approved drug with an established regulatory and clinical-use history, making it an attractive candidate for drug repurposing. In our study, fingolimod treatment was initiated after HFD and MCD models had been established. Fingolimod increased hepatic PAK1 and PPARγ phosphorylation and reduced hepatic lipid accumulation, inflammation, and fibrosis. These effects occurred without a detectable change in glucose tolerance. Together, these findings provide preclinical evidence that fingolimod may have therapeutic potential beyond its approved neurological indication and support further evaluation of PAK1 activation in MASLD/MASH.

Several limitations should be acknowledged. The mechanisms through which PAK1 regulates hepatic inflammation and fibrosis remain unresolved. Further work is also required to determine how Ser112 phosphorylation controls the nuclear distribution of PPARγ. In addition, the potential adverse effects of sustained PAK1 activation, including tumorigenic risk, require careful evaluation.

More effective PAK1 agonists and validation in large-animal models will be necessary before clinical translation.

Acknowledgements

We thank Liyan Wang, Nan Zhou and Yanwei Li from the Core Facilities, Zhejiang University School of Medicine for their technical support. The graphic images were prepared using biorender.com.

Conflict of interest

The authors declare no potential competing interests.

Funding

This work was supported by National Natural Science Foundation of China (No. 82470683); General Program of Medical Health Science and Technology Project of Zhejiang Province (No. 2025KY1026); Xu Xiao Distinguished Medical Expert Studio Fund of the First Affiliated Hospital of Zhejiang Chinese Medical University (Zhejiang Provincial Hospital of Chinese Medicine); National Natural Science Foundation of China (No. 12304256); Zhejiang Provincial Natural Science Foundation of China (No. LQ24C050005).

Availability of Data and Materials

The data that support the findings of this study are available from the corresponding author upon reasonable request.

References

1 Devarbhavi, H. *et al.* Global burden of liver disease: 2023 update. *J Hepatol* **79**, 516-537 (2023). https://doi.org:10.1016/j.jhep.2023.03.017

2 Zheng, C. *et al.* Ileitis promotes MASLD progression via bile acid modulation and enhanced TGR5 signaling in ileal CD8(+) T cells. *J Hepatol* **80**, 764-777 (2024). https://doi.org:10.1016/j.jhep.2023.12.024

3 Shah, P. A., Patil, R. & Harrison, S. A. NAFLD-related hepatocellular carcinoma: The growing challenge. *Hepatology* **77**, 323-338 (2023). https://doi.org:10.1002/hep.32542

4 Powell, E. E., Wong, V. W. & Rinella, M. Non-alcoholic fatty liver disease. *Lancet* **397**, 2212-2224 (2021). https://doi.org:10.1016/s0140-6736(20)32511-3

5 Gao, F. Q. *et al.* Stratification of adjuvant FOLFOX chemotherapy after liver transplantation for hepatocellular carcinoma. *Hepatobiliary Pancreat Dis Int* (2025). https://doi.org:10.1016/j.hbpd.2025.11.006

6 Cao, M. *et al.* Potential impact of controlling risk factors on future liver cancer deaths in China. *Chin J Cancer Res* **37**, 390-403 (2025). https://doi.org:10.21147/j.issn.1000-9604.2025.03.08

7 Targher, G., Byrne, C. D. & Tilg, H. NAFLD and increased risk of cardiovascular disease: clinical associations, pathophysiological mechanisms and pharmacological implications. *Gut* **69**, 1691-1705 (2020). https://doi.org:10.1136/gutjnl-2020-320622

8 Ferguson, D. & Finck, B. N. Emerging therapeutic approaches for the treatment of NAFLD and type 2 diabetes mellitus. *Nat Rev Endocrinol* **17**, 484-495 (2021). https://doi.org:10.1038/s41574-021-00507-z

9 Yang, M. & Liu, J. Genetic research on MASLD: New insights into cardiovascular disease and cancer risk. *iLIVER* **3** (2024). https://doi.org:10.1016/j.iliver.2024.100108

10 Zhang, X., Lau, H. C. & Yu, J. Pharmacological treatment for metabolic dysfunction-associated steatotic liver disease and related disorders: Current and emerging therapeutic options. *Pharmacol Rev* **77**, 100018 (2025). https://doi.org:10.1016/j.pharmr.2024.100018

11 Amirthalingam, M., Palanisamy, S. & Tawata, S. p21-Activated kinase 1 (PAK1) in aging and longevity: An overview. *Ageing Res Rev* **71**, 101443 (2021). https://doi.org:10.1016/j.arr.2021.101443

12 Yuan, H. *et al.* Hepatocyte-specific deletion of Cdc42 results in delayed liver regeneration after partial hepatectomy in mice. *Hepatology* **49**, 240-249 (2009). https://doi.org:10.1002/hep.22610

13 Ahn, M. *et al.* A requirement for PAK1 to support mitochondrial function and maintain cellular redox balance via electron transport chain proteins to prevent β-cell apoptosis. *Metabolism* **115**, 154431 (2021). https://doi.org:10.1016/j.metabol.2020.154431

14 Strochlic, T. I., Viaud, J., Rennefahrt, U. E., Anastassiadis, T. & Peterson, J. R. Phosphoinositides are essential coactivators for p21-activated kinase 1. *Mol Cell* **40**, 493-500 (2010). https://doi.org:10.1016/j.molcel.2010.10.015

15 Sylow, L. *et al.* Rac1 signaling is required for insulin-stimulated glucose uptake and is dysregulated in insulin-resistant murine and human skeletal muscle. *Diabetes* **62**, 1865-1875 (2013). https://doi.org:10.2337/db12-1148

16 Merz, K. E. *et al.* Changes in Skeletal Muscle PAK1 Levels Regulate Tissue Crosstalk to Impact Whole Body Glucose Homeostasis. *Front Endocrinol (Lausanne)* **13**, 821849 (2022). https://doi.org:10.3389/fendo.2022.821849

17 Lee, Y. K., Park, J. E., Lee, M. & Hardwick, J. P. Hepatic lipid homeostasis by peroxisome proliferator-activated receptor gamma 2. *Liver Res* **2**, 209-215 (2018). https://doi.org:10.1016/j.livres.2018.12.001

18 Sinha, R. A. Targeting nuclear receptors for NASH/MASH: From bench to bedside. *Liver Res* **8**, 34-45 (2024). https://doi.org:10.1016/j.livres.2024.03.002

19 Lomonaco, R. *et al.* Effect of adipose tissue insulin resistance on metabolic parameters and liver histology in obese patients with nonalcoholic fatty liver disease. *Hepatology* **55**, 1389-1397 (2012). https://doi.org:10.1002/hep.25539

20 Lee, S. M. *et al.* Hepatocyte PPARγ contributes to the progression of non-alcoholic steatohepatitis in male and female obese mice. *Cell Mol Life Sci* **80**, 39 (2023). https://doi.org:10.1007/s00018-022-04629-z

21 Baumann, A. *et al.* GW9662, a peroxisome proliferator-activated receptor gamma antagonist, attenuates the development of non-alcoholic fatty liver disease. *Metabolism* **133**, 155233 (2022). https://doi.org:10.1016/j.metabol.2022.155233

22 Zuo, S. *et al.* Lipid synthesis, triggered by PPARγ T166 dephosphorylation, sustains reparative function of macrophages during tissue repair. *Nat Commun* **15**, 7269 (2024). https://doi.org:10.1038/s41467-024-51736-5

23 Li, D. *et al.* WIP1 phosphatase is a critical regulator of adipogenesis through dephosphorylating PPARγ serine 112. *Cell Mol Life Sci* **74**, 2067-2079 (2017). https://doi.org:10.1007/s00018-016-2450-4
24 Mirdita, M. *et al.* ColabFold: making protein folding accessible to all. *Nat Methods* **19**, 679-682 (2022). https://doi.org:10.1038/s41592-022-01488-1
25 Jo, S., Kim, T., Iyer, V. G. & Im, W. CHARMM-GUI: a web-based graphical user interface for CHARMM. *J Comput Chem* **29**, 1859-1865 (2008). https://doi.org:10.1002/jcc.20945
26 Ng, Y. W. *et al.* Why an A-loop phospho-mimetic fails to activate PAK1: understanding an inaccessible kinase state by molecular dynamics simulations. *Structure* **18**, 879-890 (2010). https://doi.org:10.1016/j.str.2010.04.011
27 Hess, B., Kutzner, C., van der Spoel, D. & Lindahl, E. GROMACS 4: Algorithms for Highly Efficient, Load-Balanced, and Scalable Molecular Simulation. *J Chem Theory Comput* **4**, 435-447 (2008). https://doi.org:10.1021/ct700301q
28 Humphrey, W., Dalke, A. & Schulten, K. VMD: visual molecular dynamics. *J Mol Graph* **14**, 33-38, 27-38 (1996). https://doi.org:10.1016/0263-7855(96)00018-5
29 Huang, J. *et al.* CHARMM36m: an improved force field for folded and intrinsically disordered proteins. *Nat Methods* **14**, 71-73 (2017). https://doi.org:10.1038/nmeth.4067
30 Vanommeslaeghe, K. *et al.* CHARMM general force field: A force field for drug-like molecules compatible with the CHARMM all-atom additive biological force fields. *J Comput Chem* **31**, 671-690 (2010). https://doi.org:10.1002/jcc.21367
31 Smati, S. *et al.* Integrative study of diet-induced mouse models of NAFLD identifies PPARα as a sexually dimorphic drug target. *Gut* **71**, 807-821 (2022). https://doi.org:10.1136/gutjnl-2020-323323
32 Schuster, S., Cabrera, D., Arrese, M. & Feldstein, A. E. Triggering and resolution of inflammation in NASH. *Nat Rev Gastroenterol Hepatol* **15**, 349-364 (2018). https://doi.org:10.1038/s41575-018-0009-6
33 Li, T. *et al.* Epithelial membrane protein 1 drives hepatic stellate cell activation via the TLN1/FAK cascade in MASLD donor liver transplantation. *Mol Biomed* **6**, 116 (2025). https://doi.org:10.1186/s43556-025-00371-7
34 Frick, A. *et al.* A Novel PAK1-Notch1 Axis Regulates Crypt Homeostasis in Intestinal Inflammation. *Cell Mol Gastroenterol Hepatol* **11**, 892-907.e891 (2021). https://doi.org:10.1016/j.jcmgh.2020.11.001

35 Leistner, D. M. *et al.* Transcoronary gradients of vascular miRNAs and coronary atherosclerotic plaque characteristics. *Eur Heart J* **37**, 1738-1749 (2016). https://doi.org:10.1093/eurheartj/ehw047

36 Liu, J. *et al.* The Smad4-MYO18A-PP1A complex regulates β-catenin phosphorylation and pemigatinib resistance by inhibiting PAK1 in cholangiocarcinoma. *Cell Death Differ* **29**, 818-831 (2022). https://doi.org:10.1038/s41418-021-00897-7

37 Wu, H. *et al.* Progressive Pulmonary Fibrosis Is Caused by Elevated Mechanical Tension on Alveolar Stem Cells. *Cell* **180**, 107-121.e117 (2020). https://doi.org:10.1016/j.cell.2019.11.027

38 Jokl, E. *et al.* PAK1-dependent mechanotransduction enables myofibroblast nuclear adaptation and chromatin organization during fibrosis. *Cell Rep* **42**, 113414 (2023). https://doi.org:10.1016/j.celrep.2023.113414

39 Hu, X. *et al.* Integrated Multiomics Reveals Silencing of has_circ_0006646 Promotes TRIM21-Mediated NCL Ubiquitination to Inhibit Hepatocellular Carcinoma Metastasis. *Adv Sci (Weinh)* **11**, e2306915 (2024). https://doi.org:10.1002/advs.202306915

40 Ye, Q. *et al.* Ubiquitin-specific protease 22 promotes tumorigenesis and progression by an FKBP12/mTORC1/autophagy positive feedback loop in hepatocellular carcinoma. *MedComm (2020)* **4**, e439 (2023). https://doi.org:10.1002/mco2.439

41 Chen, L. *et al.* Ivermectin suppresses tumour growth and metastasis through degradation of PAK1 in oesophageal squamous cell carcinoma. *J Cell Mol Med* **24**, 5387-5401 (2020). https://doi.org:10.1111/jcmm.15195

42 Chow, H. Y. *et al.* Development and Utility of a PAK1-Selective Degrader. *J Med Chem* **65**, 15627-15641 (2022). https://doi.org:10.1021/acs.jmedchem.2c00756

43 Wang, K. *et al.* Ivermectin induces PAK1-mediated cytostatic autophagy in breast cancer. *Autophagy* **12**, 2498-2499 (2016). https://doi.org:10.1080/15548627.2016.1231494

44 Wang, K. *et al.* PAK1 inhibition increases TRIM21-induced PD-L1 degradation and enhances responses to anti-PD-1 therapy in pancreatic cancer. *Biochim Biophys Acta Mol Basis Dis* **1870**, 167236 (2024). https://doi.org:10.1016/j.bbadis.2024.167236

45 Tate, T. *et al.* Pparg signaling controls bladder cancer subtype and immune exclusion. *Nat Commun* **12**, 6160 (2021). https://doi.org:10.1038/s41467-021-26421-6

46 Li, L. *et al.* Hepatocyte-specific Nrf2 deficiency mitigates high-fat diet-induced hepatic steatosis: Involvement of reduced PPARγ expression. *Redox Biol* **30**, 101412 (2020). https://doi.org:10.1016/j.redox.2019.101412

47 Cui, K. *et al.* Ferulic Acid and P-Coumaric Acid Synergistically Attenuate Non-Alcoholic Fatty Liver Disease through HDAC1/PPARG-Mediated Free Fatty Acid Uptake. *Int J Mol Sci* **23** (2022). https://doi.org:10.3390/ijms232315297
48 Zhao, L. *et al.* CD36 palmitoylation disrupts free fatty acid metabolism and promotes tissue inflammation in non-alcoholic steatohepatitis. *J Hepatol* **69**, 705-717 (2018). https://doi.org:10.1016/j.jhep.2018.04.006
49 Zeng, H. *et al.* CD36 promotes de novo lipogenesis in hepatocytes through INSIG2-dependent SREBP1 processing. *Mol Metab* **57**, 101428 (2022). https://doi.org:10.1016/j.molmet.2021.101428
50 Li, Y. *et al.* CD36 favours fat sensing and transport to govern lipid metabolism. *Prog Lipid Res* **88**, 101193 (2022). https://doi.org:10.1016/j.plipres.2022.101193
51 Li, X. C. *et al.* Canagliflozin alleviates pulmonary hypertension by activating PPARγ and inhibiting its S225 phosphorylation. *Acta Pharmacol Sin* **45**, 1861-1878 (2024). https://doi.org:10.1038/s41401-024-01286-9
52 Haas, B. *et al.* Sulfonylureas exert antidiabetic action on adipocytes by inhibition of PPARγ serine 273 phosphorylation. *Mol Metab* **85**, 101956 (2024). https://doi.org:10.1016/j.molmet.2024.101956
53 Terra, M. F. *et al.* Obesity-Linked PPARγ Ser273 Phosphorylation Promotes Beneficial Effects on the Liver, despite Reduced Insulin Sensitivity in Mice. *Biomolecules* **13** (2023). https://doi.org:10.3390/biom13040632
54 Yang, N. *et al.* Blockage of PPARγ T166 phosphorylation enhances the inducibility of beige adipocytes and improves metabolic dysfunctions. *Cell Death Differ* **30**, 766-778 (2023). https://doi.org:10.1038/s41418-022-01077-x
55 Hu, E., Kim, J. B., Sarraf, P. & Spiegelman, B. M. Inhibition of adipogenesis through MAP kinase-mediated phosphorylation of PPARgamma. *Science* **274**, 2100-2103 (1996). https://doi.org:10.1126/science.274.5295.2100
56 Kappos, L. *et al.* A placebo-controlled trial of oral fingolimod in relapsing multiple sclerosis. *N Engl J Med* **362**, 387-401 (2010). https://doi.org:10.1056/NEJMoa0909494
57 Cohen, J. A. *et al.* Oral fingolimod or intramuscular interferon for relapsing multiple sclerosis. *N Engl J Med* **362**, 402-415 (2010). https://doi.org:10.1056/NEJMoa0907839

Figure legends

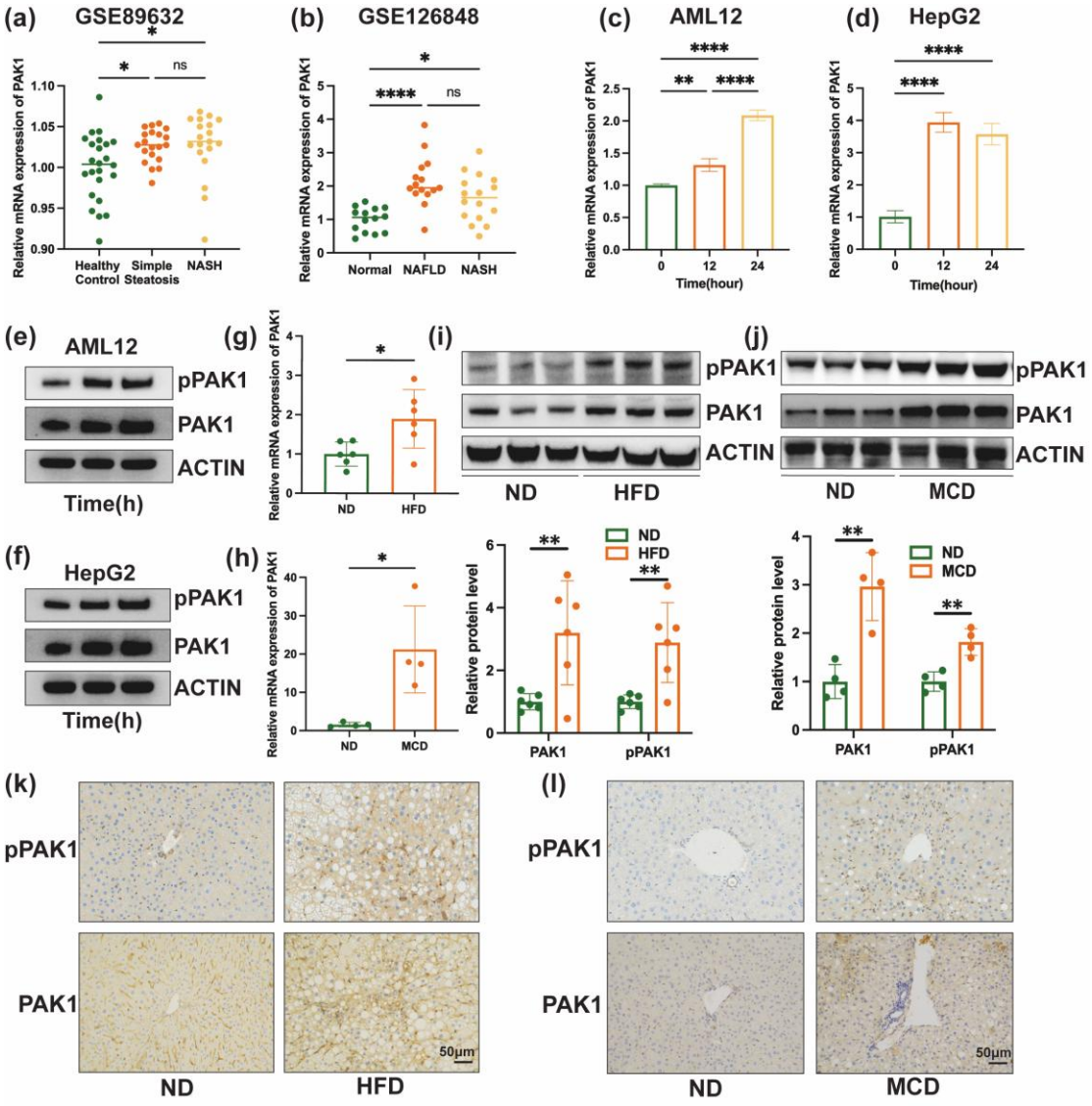


Fig. 1. PAK1 expression is increased in livers and hepatocytes with steatosis. (a,b) The mRNA levels of PAK1 in livers of healthy human, patients with simple liver steatosis or MASH from GEO database (GSE89632,GSE126848). AML12 and HepG2 cells were treated with 400 μM oleic acid (OA) for 0,12,24 hours and the mRNA levels of PAK1 were determined by RT-qPCR in AML12 **(c)** and HepG2 **(d)**. The protein levels of PAK1 in AML12 **(e)** and HepG2 **(f)** were determined by western blotting. The mRNA levels of PAK1 in mouse livers after 12 weeks of normal diet (ND) or high fat diet (HFD) treatment (n=6) **(g)** and 6 weeks of normal diet (ND) or methionine-choline-

deficient diet (MCD) (n=4) **(h)** were determined by RT-qPCR. The protein levels of PAK1 in mouse livers in HFD **(i)** or MCD **(j)** models were determined by western blotting. Representative immunohistochemical staining images of PAK1 expression in mouse livers after HFD **(k)** or MCD **(l)** diet for 12 or 6 weeks were showed. ns, not significant; *,$p<0.05$;**,$p<0.01$; ****, $p<0.0001$.

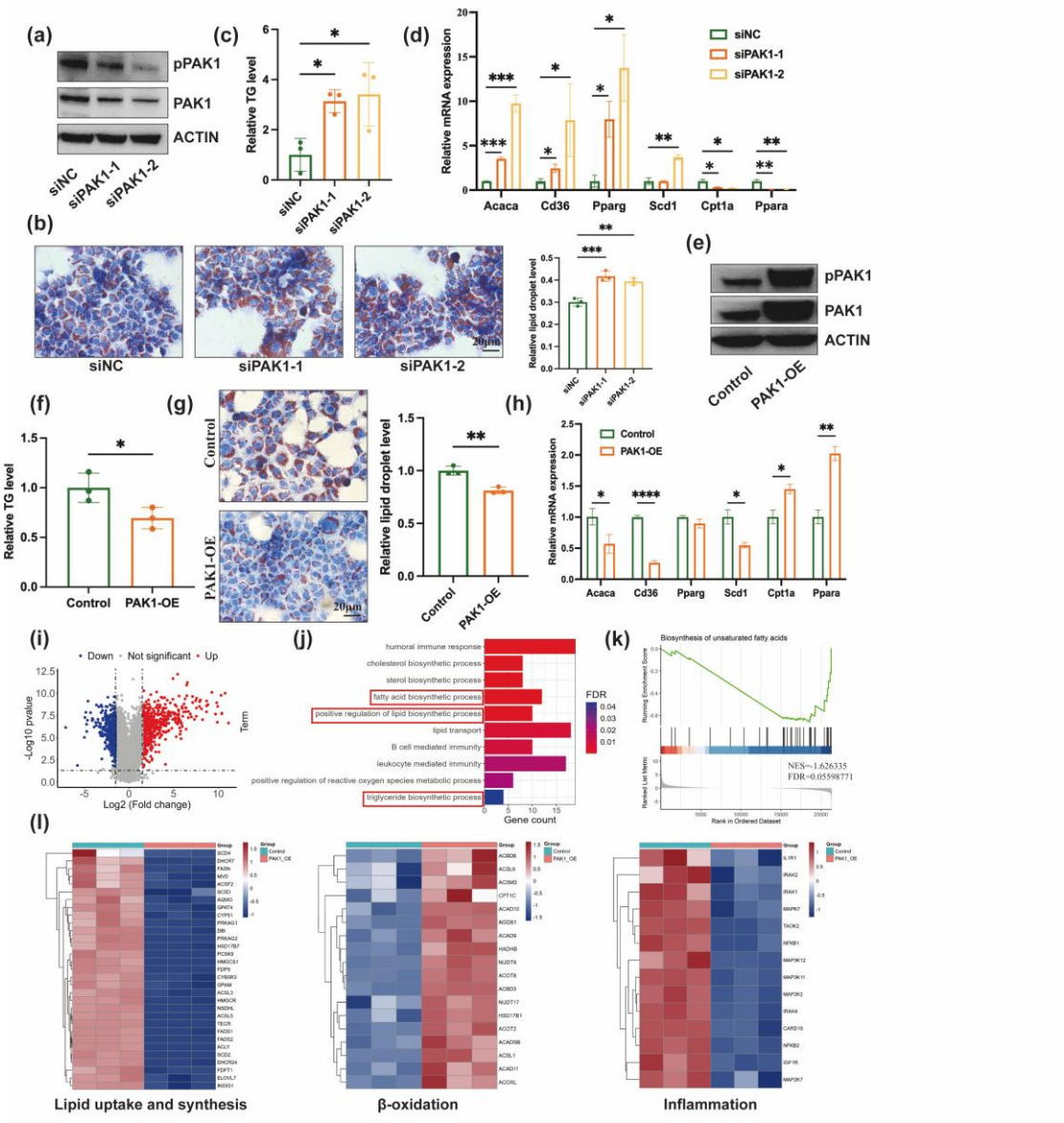


Fig. 2. PAK1 suppresses lipid accumulation in hepatocytes. (a) The PAK1 protein expression in AML12 cells transfected with siNC or siPAK1-1and siPAK1-2. **(b)** Intracellular triglyceride (TG) level in the indicated groups after 400μM OA treatment for 24 hours. **(c)** Representative Oil Red O staining images showing lipid accumulation in AML12 cells transfected with siRNA followed by 400μM OA treatment for 24 hours. **(d)** Relative mRNA levels of genes related to lipid synthesis (stearoyl-Coenzyme A desaturase 1 [Scd1], cluster of differentiation 36 [Cd36], peroxisome proliferator activated receptor gamma [Pparg], acetyl coenzyme A carboxylase alpha [Acaca]), β-oxidation (carnitine palmitoyltransferase 1a [Cpt1a], peroxisome proliferator activated receptor

alpha [Ppara]) in AML12 cells transfected with siRNA. **(e)** The PAK1 protein expression in AML12 cells infected with Control or PAK1 overexpressing lenti-virus. Relative intracellular TG levels **(f)** were assessed and representative Oil Red O staining images **(g)** were showed in the indicated groups. **(h)** Relative mRNA levels of genes related to lipid synthesis and β-oxidation in AML12 cells infected with lenti-virus. **(i)** Clustering analysis identified differentially expressed genes. KEGG **(j)** and GSEA **(k)** enrichment analysis showed these genes were enriched in pathways related to metabolism and inflammation. **(l)** Heatmap shows the leading edge subsets of genes related to lipid metabolism and inflammation. *,$p<0.05$;**,$p<0.01$; ***, $p<0.001$; ****, $p<0.0001$.

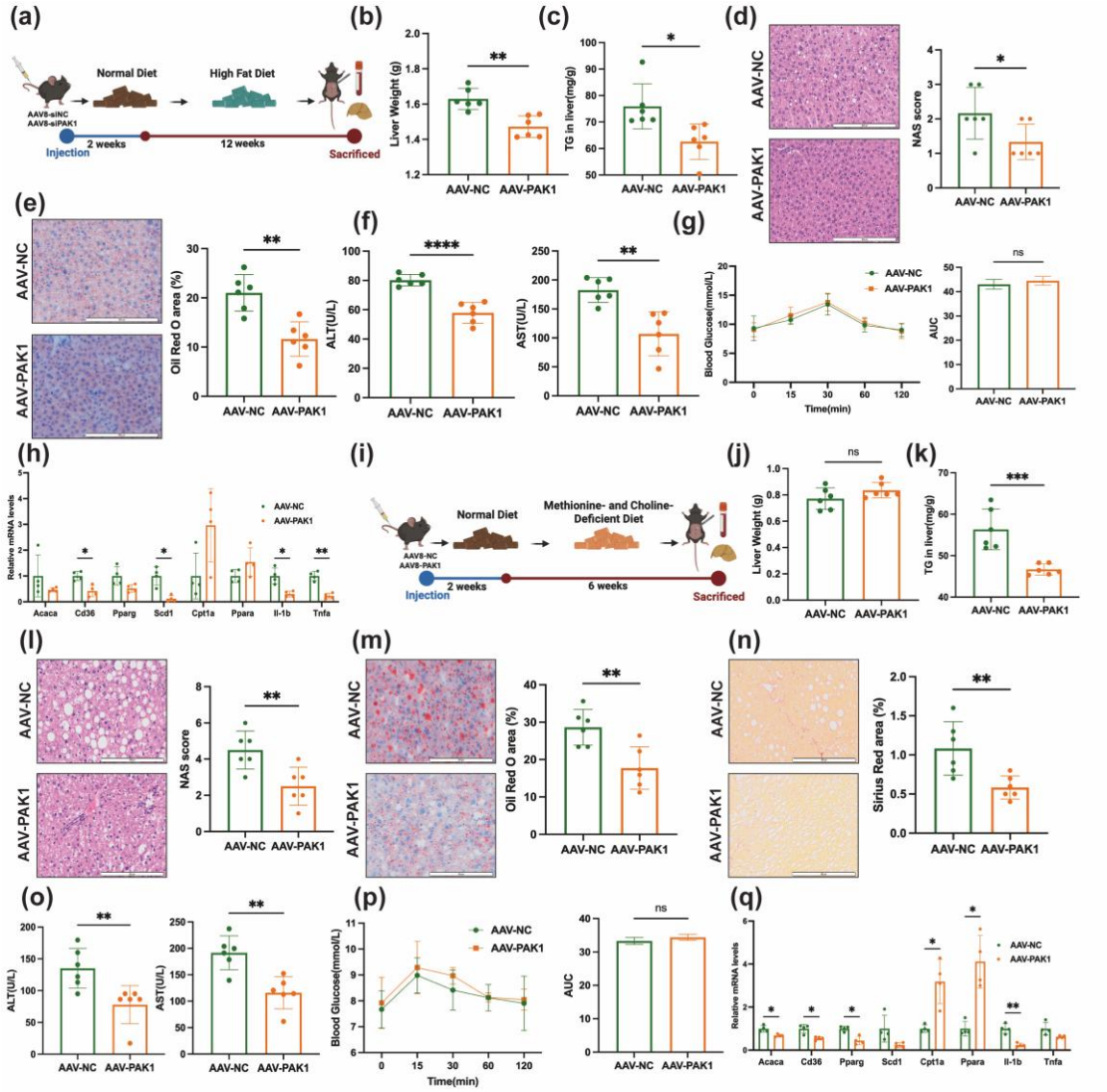


Fig. 3. PAK1 alleviates HFD and MCD diet-induced MASLD/MASH progression. (a) Scheme of constructing HFD models. **(b)** Liver weight (LW) of mice injected with control or overexpression adeno-associated virus followed by 2 weeks of normal diet and 12 weeks of high fat diet (n=6) was presented. **(c)** Liver TG contents of mice of the indicated groups. Representative Hematoxylin and Eosin (H&E) **(d)** , Oil red O staining **(e)** of HFD models. The NAS score was determined by pathologists. Oil red O area was determined by image J. **(f)** Serum alanine aminotransferase (ALT) and aspartate aminotransferase (AST) contents of the indicated groups were showed. **(g)** Blood glucose were measured at indicated time in glucose tolerance test (GTT) and the corresponding area under the curve (AUC) of GTT was showed. **(h)** Relative mRNA level of genes related to lipid

synthesis (Acaca, Cd36, Pparg, Scd1) , β-oxidation (Ppara, Cpt1a) and inflammation (Il-1b, Tnfa) in the liver tissues from indicated groups were showed. **(i)** Scheme of constructing MCD models. **(j)** Liver weight (LW) of mice injected with control or overexpression adeno-associated virus followed by 2 weeks of normal diet and 6 weeks of methionine-choline-deficient diet (n=6) was presented. **(k)** Liver TG contents of mice of the indicated groups. Representative Hematoxylin and Eosin (H&E) **(l)** , Oil red O staining **(m),** Sirius Red staining of MCD models. The Sirius Red staining area was determined by image J. **(o)** Serum ALT and AST contents of the indicated groups were showed. **(p)** Blood glucose were measured at indicated time in GTT and the AUC of GTT was showed. **(q)** Relative mRNA level of genes related to lipid synthesis, β-oxidation and inflammationin the liver tissues from indicated groups were showed.*,$p<0.05$;**,$p<0.01$; ****, $p<0.0001$.

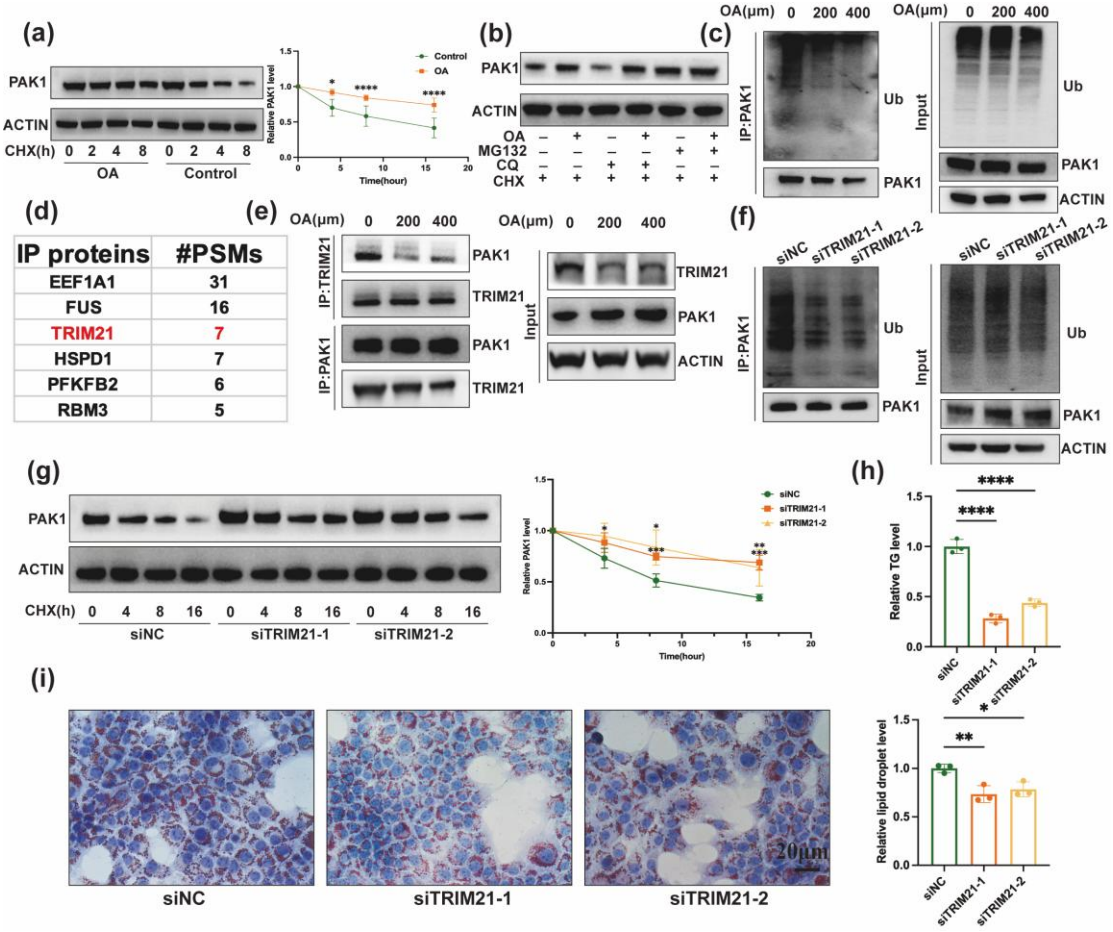


Fig. 4.TRIM21 mediates degradation of PAK1 under metabolic challenge. (a) Half-life assays of PAK1. Samples were treated with OA (400μM) and CHX (100μM) and then were collected at indicated time. **(b)** The protein level of PAK1 in AML12 cells treated with MG132 (50μM), Chlq (50μM) , CQ(100μM) or Dmethylsulfoxide control. **(c)** CO-IP results showed the effect of OA on ubiquitination of PAK1 after MG132 (50μM) and OA treatment. **(d)** IP-MS results showed proteins interacting with PAK1. **(e)** CO-IP performed the interaction between PAK1 and TRIM21 in AML12 cells treated with indicated concentration. **(f)** CO-IP detected the ubiquitin combined with PAK1 after TRIM21 knockdown. **(g)** Half-life assays of PAK1. Samples were treated with OA (400μM) and CHX (100μM) and then were collected at indicated time. Lipid accumulation after TRIM21 knockdown and treatment with OA (400μM) for 24h was compared by intracellular

TG measurement **(h)** and Oil Red staining **(i)**. *,p<0.05;**,p<0.01; ***, p<0.001； ****, p<0.0001.

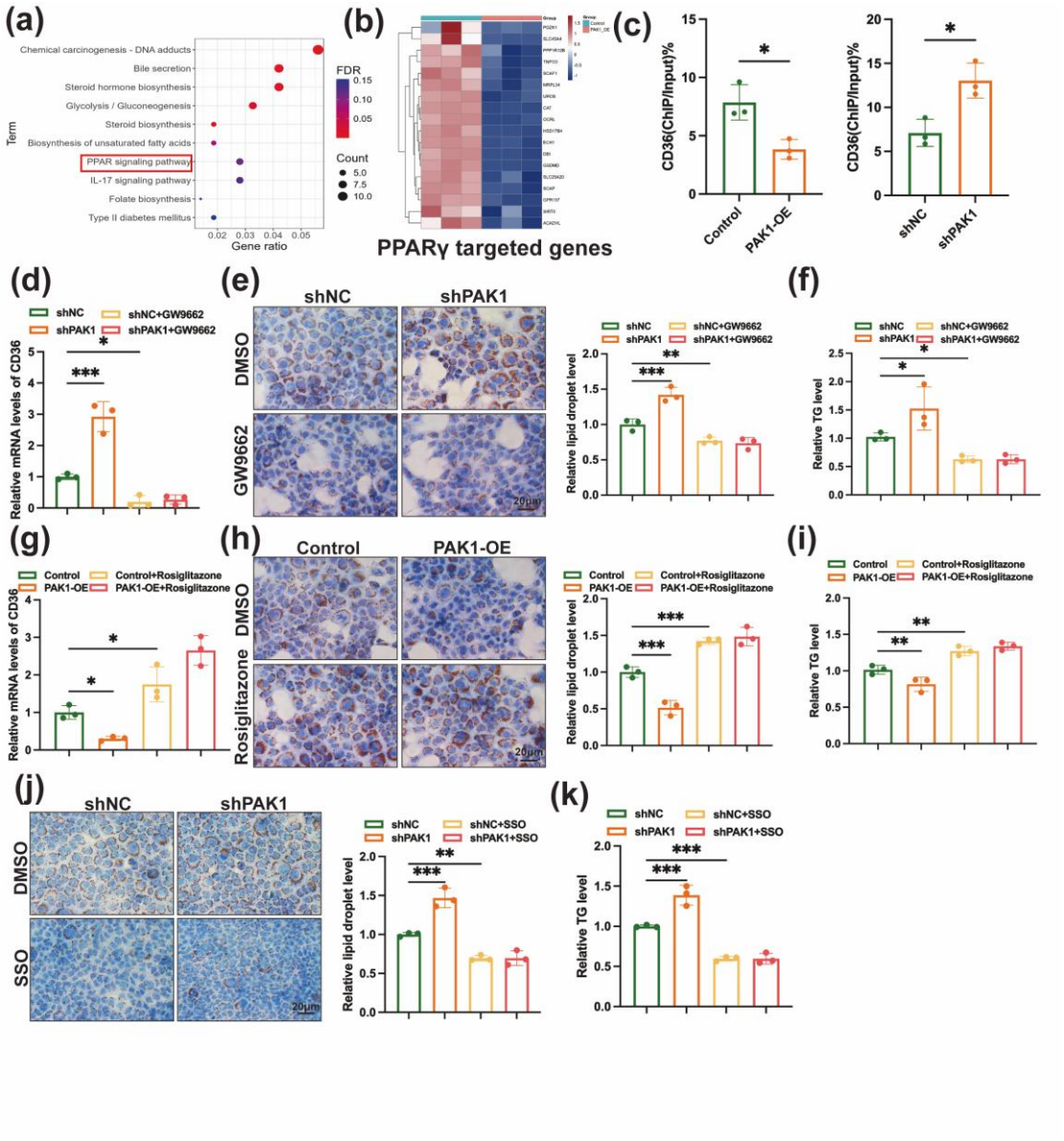


Fig. 5. PAK1 suppresses lipid accumulation through PPARγ/CD36. (a) GO enrichment analysis showed downregulated genes in PAK1-OE AML12 cells were enriched in PPAR pathway. **(b)** Heatmap of differentially expressed genes on PPAR signaling pathway between control and PAK1-OE. **(c)** Ch-IP assay showed the combination of PPARγ and promoters of CD36. **(d)** The mRNA levels of CD36 in AML12 cells infected with shNC or shPAK1 lenti-virus and then treated with either GW9662 (10μM) or dimethylsulfoxide. **(e)** Representative Oil Red O staining images showing lipid accumulation of indicated groups. **(f)** Intracellular TG level of indicated groups. **(g)** The mRNA levels of CD36 in AML12 cells infected with Control or PAK1-OE lenti-virus and then

treated with either Rosiglitazone (20μM) or dimethylsulfoxide. **(h)** Representative Oil Red O staining images showing lipid accumulation of indicated groups. **(i)** Intracellular TG level of indicated groups. **(j)** Representative Oil Red O staining images of AML12 cells infected with shNC or shPAK1 lenti-virus and then treated with sulfosuccinimidyl oleate (SSO) (100μM) or dimethylsulfoxide. **(k)** Intracellular TG level of indicated groups. *,$p<0.05$;**,$p<0.01$; ***, $p<0.001$; ****, $p<0.001$.

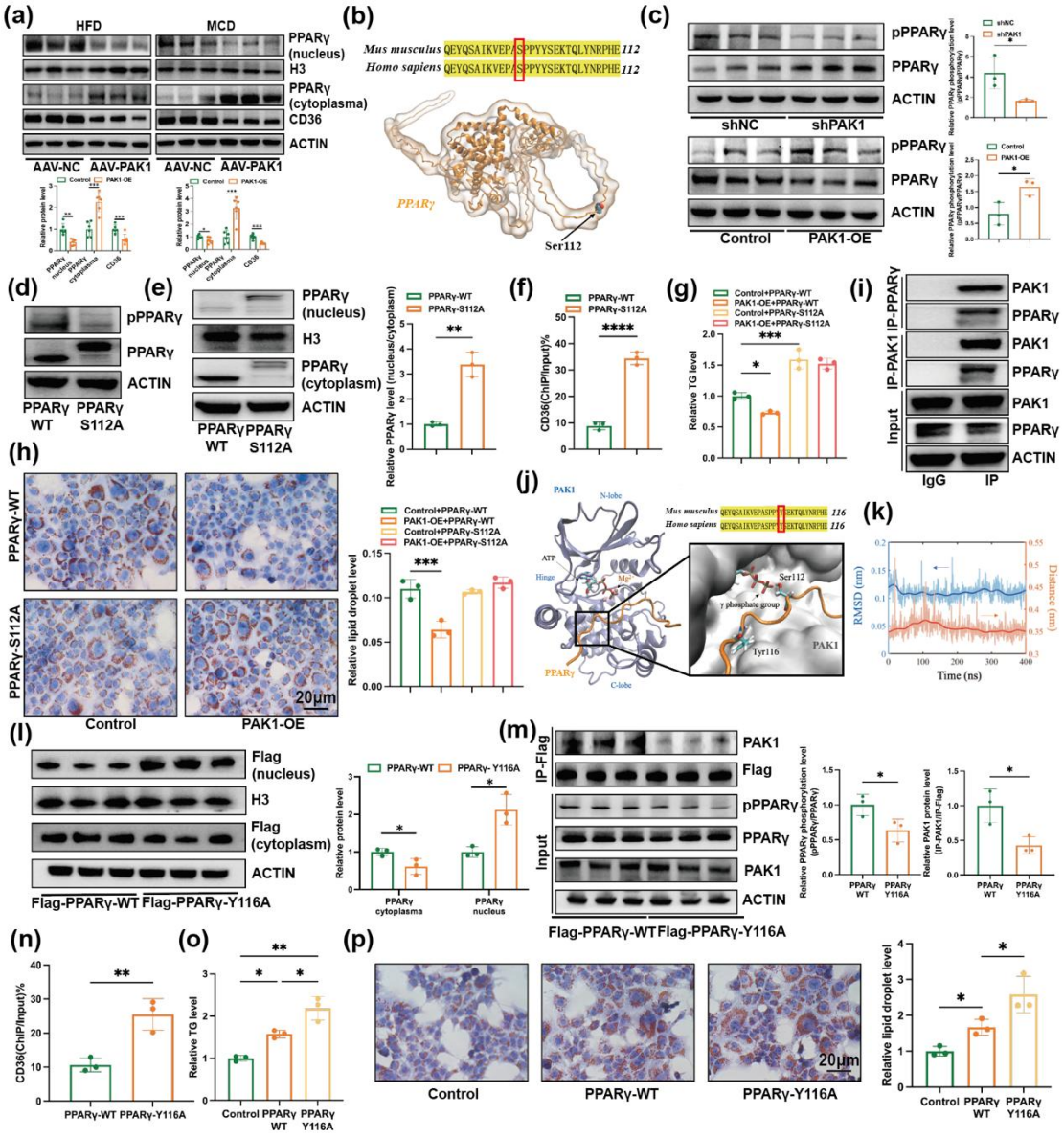


Fig. 6. PAK1 binds to PPARγ at Tyr116 to facilitate its phosphorylation at Ser112. (a) The protein levels of nuclear and cytoplasma PPARγ and CD36 in livers of mice injected with control or overexpression adeno-associated virus followed by HFD or MCD treatment. **(b)** The 3D structure of mouse PPARG. Its phosphorylation site Ser112 is indicated. **(c)** The phosphorylation levels of PPARγ in AML12 cells infected with overexpression or knockdown lenti-virus. **(d)** The levels of phosphorylated and total PPARγ in AML12 transfected with PPARγ (WT) or mCherry-PPARγ (S112A) plasmids. **(e)** The protein levels of nuclear and cytoplasma PPARγ of indicated groups. **(f)** Ch-IP assay showed the combination of PPARγ and promoters of CD36. **(g)** Intracellular TG level

of indicated groups. **(h)** Representative Oil Red O staining images showing lipid accumulation of AML12 cells infected with Control or PAK1-OE lenti-virus and then treated with PPARγ (WT) or PPARγ (S112A) plasmids. **(i)** CO-IP performed the interaction between PAK1 and PPARγ in AML12 cells. **(j)** Snapshot of a representative complex formed by mouse PAK1 and PPARγ and a detailed look of the binding mode. **(k)** Time evolution of root-mean-square deviation (RMSD) of peptide segment SPPYY (i.e., the segment ranging from Ser112 to Tyr116 of the substrate) and the distance between hydroxyl group of Ser112 and γ phosphate group of ATP. **(l)** The nuclear and cytoplasm protein level of PPARγ in AML12 cells transfected with PPARγ-Y116A plasmid and its control. **(m)** CO-IP performed the interaction between PAK1 and indicated PPARγ, and the levels of P-PPARγ, PPARγ and CD36 were showed. **(n)** Ch-IP assay showed the combination of PPARγ and promoters of CD36. Intracellular TG level **(o)** and representative Oil Red O staining images **(p)** were got in AML12 cells transfected with indicated plasmids after 24h OA (400μM) treatment.

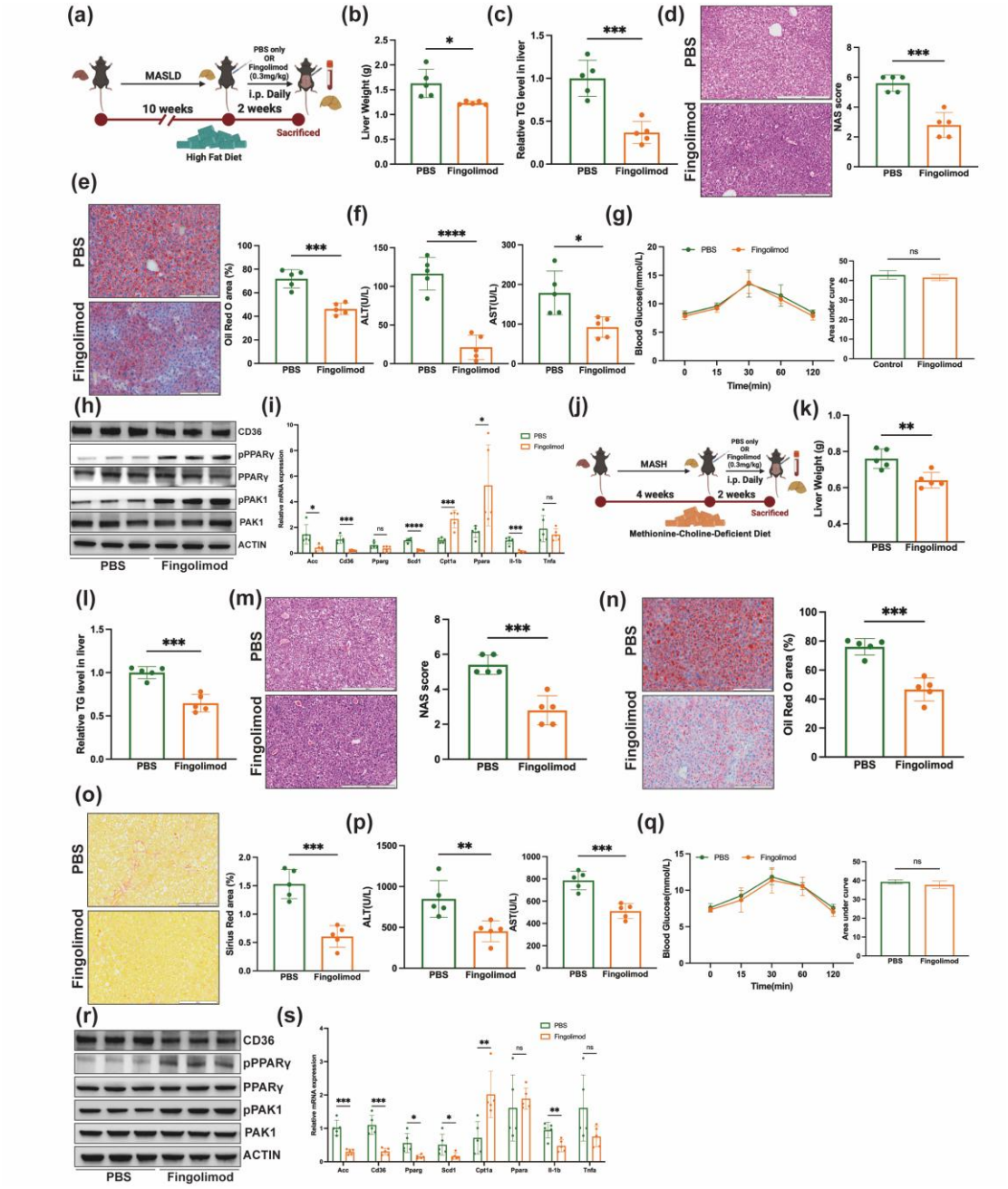


Fig. 7. PAK1 agonists Fingolimod protects against MASLD/MASH which can be reversed by PPARγ activation. (a) Scheme of constructing HFD injected with indicated drugs. **(b)** Liver weight (LW) of mice (n=5) was presented. **(c)** Liver TG contents of mice of the indicated groups. Representative Hematoxylin and Eosin (H&E) **(d)** , Oil red O staining **(e)** of HFD models. NAS score was determined by pathologists, Oil red O area was determined by image J. **(f)** Serum alanine aminotransferase (ALT) and aspartate aminotransferase (AST) contents of the indicated groups were

showed. **(g)** Blood glucose were measured at indicated time in glucose tolerance test (GTT) and the corresponding area under the curve (AUC) of GTT. **(h)** The protein levels of CD36, phosphorylated and total PPARγ, phosphorylated and total PAK1 in liver tissues. **(i)** Relative mRNA level of genes related to lipid synthesis (Acc, Cd36, Pparg, Scd1) , β-oxidation (Ppara, Cpt1a) and inflammation (Il-1b, Tnfa) in the liver tissues from indicated groups were showed. **(j)** Scheme of constructing MCD injected with indicated drugs. **(k)** LW of mice fed methionine-choline-deficient diet (n=5) was presented. **(l)** Liver TG contents of mice of the indicated groups. Representative Hematoxylin and Eosin (H&E) **(m)** , Oil red O staining **(n)** of MCD models. Sirius Red area was determined by image J. **(p)** Serum ALT and AST contents of the indicated groups were showed. **(q)** Blood glucose were measured at indicated time in GTT and the corresponding AUC of GTT. **(r)** The protein levels of CD36, phosphorylated and total PPARγ, phosphorylated and total PAK1 in liver tissues. **(s)** Relative mRNA level of genes related to lipid synthesis , β-oxidation and inflammation in the liver tissues from indicated groups were showed.*,$p<0.05$;**,$p<0.01$; ***,$p<0.001$;****, $p<0.0001$.

Supplementary Files

This is a list of supplementary files associated with this preprint. Click to download.

- uncroppedGelsandBlotsimages.pdf
- Supportinginformation.docx